Journal of
Applied Crystallography
ISSN 0021-8898

Received 26 October 2010
Accepted 27 January 2011

Near-surface relaxation structure of annealed block copolymer film on Si substrates examined by grazing-incidence small-angle scattering utilizing soft X-rays

Hiroshi Okuda,[a]* Kohki Takeshita,[a] Shojiro Ochiai,[a] Shin-ichi Sakurai[b] and Yoshinori Kitajima[c]

[a]Department of Materials Science and Engineering, Kyoto University, Yoshida Honmachi, Sakyo-ku, Kyoto, 606-8501, Japan, [b]Department of Polymer Science and Engineering, Kyoto Institute of Technology, Matsugasaki, Sakyo-ku, Kyoto, 606-8585, Japan, and [c]Photon Factory, KEK, Oho Tsukuba 305-0801, Japan. Correspondence e-mail: okuda@materials.mbox.media.kyoto-u.ac.jp

Two-dimensional grazing-incidence small-angle X-ray scattering (GISAXS) measurements of SEBS8 block copolymer films deposited on Si(001) substrates have been performed to demonstrate depth-sensitive GISAXS utilizing soft X-rays of 1.77 keV. Remarkable elongation of the Bragg spots in the q_z direction, corresponding to microphase separation, was observed for an angle of incidence close to the critical angle. The elongation was explained in terms of the penetration depth, which limits the effective size in the direction perpendicular to the sample surface. Lattice distortion near the surface was confirmed.

1. Introduction

Self-organized nanostructures formed by microphase separation on substrates attract attention because of their potential use as templates for nanocomposite structures (Harrison *et al.*, 2004; Park *et al.*, 2007; Matsen & Bates, 1996). For templates, it is important that the film layers have the intended uniform and well defined structure. From this viewpoint, nondestructive examination of the nanostructure distribution near the surface is an important step in the design of an optimal process to control the nanostructures of thin films, since surface- or interface-related ordering or disordering can occur for thin block copolymer films depending on the preparation method (Turner *et al.*, 1994; Huinink *et al.*, 2001; Park *et al.*, 2006). Grazing-incidence small-angle X-ray scattering (GISAXS) has been applied extensively to examine thin polymer films and their composites coated on Si substrates (Müller-Buschbaum *et al.*, 1999; Smilgies *et al.*, 2002; Jin *et al.*, 2007). This work has been extended to include various scales, from microbeam GISAXS/ultra-small-angle X-ray scattering (Roth *et al.*, 2003; Naudon *et al.*, 2000) for large structures, to grazing-incidence small- and wide-angle X-ray scattering/wide-angle X-ray scattering (Sasaki *et al.*, 2007; Perlich *et al.*, 2010) for atomic scales in reciprocal space. From a real-space perspective, the examination of nanostructures in microscopic spatial resolution has been achieved by a microbeam/nanobeam technique (Kuhlmann *et al.*, 1999; Roth *et al.*, 2007), which is effective in avoiding the effects of local curvature. However, the spatial resolution of the microbeam was not sufficient to allow the determination of structural changes within a few tens of nanometres from the surface, and the preparation of cross-sectional slices of soft materials samples was difficult. In the direction perpendicular to the substrate, depth-sensitive analysis might be achieved by controlling the penetration depth (Tolan, 1999; Singh & Groves, 2009; Mukhopadhyay et al., 2010) or, for the well defined multilayer case, by controlling the angle of incidence so that the electric field is enhanced at a specific depth of interest (Babboneau et al., 2009). Controlling the angle of incidence around the critical angle is a simple way to change the penetration depth. It is not difficult for synchrotron radiation beamlines to control the incident angle with much better resolution than the magnitude of the critical angle, even for hard X-rays above 10 keV. However, if the surface of the sample is not ideal, e.g. owing to the presence of a meniscus, surface undulation or surface defects, a small critical angle becomes a serious problem when determining the penetration depth precisely in the actual measurements. This is more serious for harder X-rays, having smaller critical angles and smaller absorption cross sections. In this respect, using soft X-rays has an advantage over hard X-rays with precise optical control. Very soft X-rays close to the K-absorption edge of C have been used by Wang et al. (2005) and Ade & Hitchcock (2008) for reflectivity/diffuse scattering and imaging measurements. In the present work, in contrast, relatively harder X-rays of about 1.77 keV have been used to measure the GISAXS pattern of the self-organized structure of a SEBS triblock copolymer film deposited on an Si substrate, because the magnitude of the expected penetration depth is convenient for this material.

2. Experimental

The samples were prepared by spin coating of a 5 wt% toluene solution of polystyrene-block-poly(ethylenebutylene)-block-

polystyrene (SEBS8) triblock copolymer (provided by Asahi Chemicals Corporation) on Si substrates. The number-average molecular weight (M_n) was 6.7×10^4, with a volume fraction of polystyrene blocks of 0.084 and polydispersity index (M_w/M_n) of 1.04. The sample was annealed at 413 K for 28.8 ks to form a three-dimensional self-organized structure. This heat treatment of the bulk sample yields a body-centered cubic (b.c.c.) lattice composed of 7.7 nm spherical cores as a result of microphase separation (Kim *et al.*, 1999). The film thickness after annealing was 372 nm as measured by an ellipsometer.

GISAXS measurements were performed at BL-11B, a bending-magnet soft-X-ray beamline at the Photon Factory, High Energy Accelerator Organization, Tsukuba, Japan. The incident X-rays are monochromated by an InSb double-crystal monochromator to a photon energy of 1.77 keV and recorded by an image plate (Okuda *et al.*, 2009). Fig. 1 shows a schematic illustration of the present measurements. The guard slits, sample stage and image plate were aligned in the same vacuum chamber. The camera length was typically 350 mm in the present measurements. Since the photon energy is less than one-quarter of that of conventional GISAS, about 8.26 keV, the camera length required to cover the necessary scattering vector is about a quarter of that required by conventional GISAS experiments performed with Cu $K\alpha$ radiation. The incident angle, α_i, was controlled by monitoring the position of the specular spot on the image plate. In the present measurements, the incident angle was chosen to be between 0.6 and 1.0°. For comparison, GISAXS measurements at 8.26 keV were made at beamline 15A of the same facility using a cooled CCD with a 6 inch (∼15 cm) image intensifier.

3. Results and discussion

GISAXS patterns of the as-deposited and annealed samples obtained for hard X-rays at 8.26 keV with $\alpha_i = 0.125°$ are shown in Fig. 2. It is clearly seen that the as-spin-cast sample shows only a diffuse peak, and after annealing at 413 K for 28.8 ks, the GISAXS pattern shows sharp Bragg spots corresponding to the lattice order of microphase separation as reported for transmission SAXS (Kim *et al.*, 1999; Sakurai *et al.*, 2005). The distribution of the spots is rather complex at 8.26 keV because the incident angle is very small, giving transmission Bragg spots (encircled) at the sample edge in addition to the Born term of GISAXS; furthermore, the waves reflected at the Si substrate, as described by the three correction terms used in standard GISAS analysis (Rauscher *et al.*, 1995), give extra spots. For example, the encircled spots in Fig. 2(*b*) are those corresponding to the transmitted wave, which can be used as a guide to specify the average spatial arrangement of cores in the sample. The GISAXS pattern of the annealed sample shows many extra spots, which do not fit the peak position in the kinematical interpretation. Such extra Bragg spots and strong Yoneda lines in the GISAXS profile appear because hard X-rays penetrate deep enough to illuminate the whole film, *i.e.* the GISAXS pattern represents the average structure over all of the polymer film. The reflected beam from the interface of the film/Si substrate is not negligible when interpreting the pattern in this case.

Since the density of the polymer film depends on the preparation conditions and thickness, the density has been evaluated using the critical angle of specular reflectivity measurements using Cu $K\alpha_1$ radiation. The real part of the refractive index at 8.26 keV was determined as $\delta = 3.1 \times 10^{-6}$, corresponding to a density of $\rho = 0.77$ g cm^{-3} using the chemical composition of the sample and the reported atomic scattering factor at $q = 0$ (Chantler *et al.*, 2005). The refractive indices at 1.77 keV were estimated from the reported atomic scattering factors at that energy and the density as determined by the reflectivity measurements described above. The critical angle at 1.77 keV was 0.64°. The penetration depth under the experimental conditions was calculated as

$$\Lambda^{-1} = \left\{2k^2\left[\left(\alpha_c^2 - \alpha_i^2\right)^2 + 4\beta^2\right]^{1/2} + \left(\alpha_c^2 - \alpha_i^2\right)^2\right\}^{1/2}, \qquad (1)$$

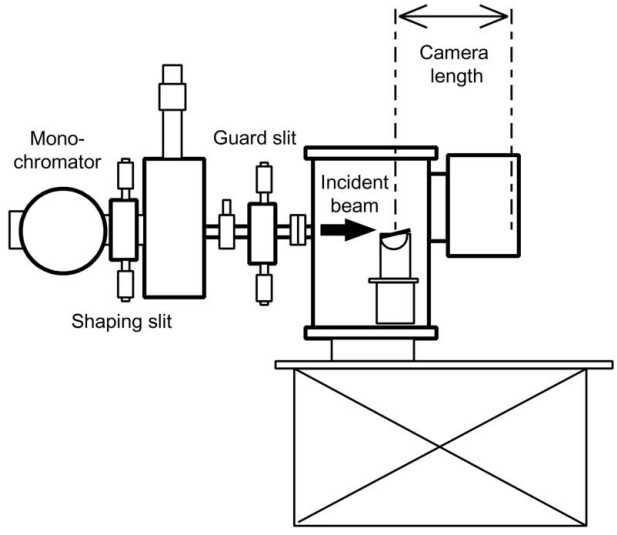

Figure 1
Schematic illustration of the present measurements at BL-11B, Photon Factory. All the components are installed in vacuum without air gap up to the detector.

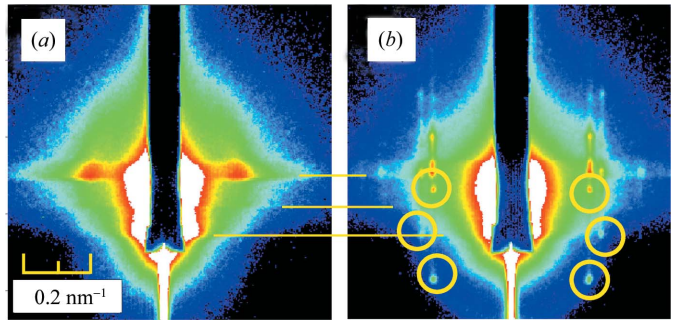

Figure 2
GISAXS pattern of the as-cast (*a*) and annealed (*b*) SEBS film obtained with hard X-rays with the same angle of incidence of 0.125°. The three horizontal lines are q_z for the direct beam, the sample horizon and the specular spot (respectively, from the bottom).

where k is the magnitude of the wavevector, α_c is the critical angle, α_i the incident angle and β the imaginary part of the refractive index. In the present work, the intended depth resolution is coarser than the penetration depth for total reflection. Fig. 3 gives the penetration depth, Λ, of the X-rays at 1.77 keV calculated for the SEBS film. Since the critical angle and the attenuation coefficient are much larger than those for hard X-rays, better control of penetration depth is expected for depth-sensitive GISAXS measurements. The arrows shown in the figure are the measurement conditions of the present GISAXS experiments at 1.77 keV. A clear difference is expected between the conditions at around the critical angle of 0.64° and those well above it.

Fig. 4 shows a series of GISAS patterns obtained for angles of incidence from 0.61 to 0.96°. Figs. 4(*a*)–4(*d*) correspond to the angles shown by arrows in Fig. 3. As shown in Fig. 3, the expected penetration depth changes from about 22 nm at 0.64° to 420 nm at 0.96°. Considering that the lattice constant of the microphase separation is about 32 nm, it is expected that the penetration depth can be controlled from about the nearest-neighbor distance of the lattice to the full film thickness. The condition that the maximum penetration depth in the present measurements is about the film thickness implies that the scattering pattern can be interpreted basically as a kinematical diffraction pattern. Remarkable elongation of the Bragg spots in the q_z direction is observed for the smaller incident angle, and peaks having the same q_y but different q_z eventually overlap each other. The FWHM in the q_y direction, on the other hand, does not change significantly with the angle of incidence. Under the present conditions, GISAXS measurements at 8.26 keV suggest that the Bragg spots are sharp in both the q_z and the q_y directions when the X-rays penetrate the whole SEBS film. This suggests that the broadening can be explained by the change in the penetration depth with the angle of incidence. Such broadening may be explained either by the size effect or by disordering of the lattice near the surface. Since the broadening is observed mainly in the q_z direction, the size effect is examined first. When the size, L, of a crystal that contributes to diffraction is limited, the truncation effect is estimated by the width, Δq, of the Laue function. A simple estimate of $L = 2\pi/\Delta q$, where Δq is the full width at half-maximum (FWHM) of the Bragg spot in the q_z direction, gives a result of the same order of magnitude as the penetration depth. This estimate is improved by taking into account the fact that the wave that contributes to the diffraction decays exponentially, not by truncation, in the present situation.

Fig. 5 shows the change of the FWHM of the Bragg spot marked by arrows in Fig. 4. As expected from Fig. 4, the FWHM in the q_z direction decreases monotonically as the incident angle increases. The peak broadening can be seen as a measure of the depth sensitivity of the GISAXS measurement. A simple calculation of the Laue function with an attenuation decay in the depth direction gives

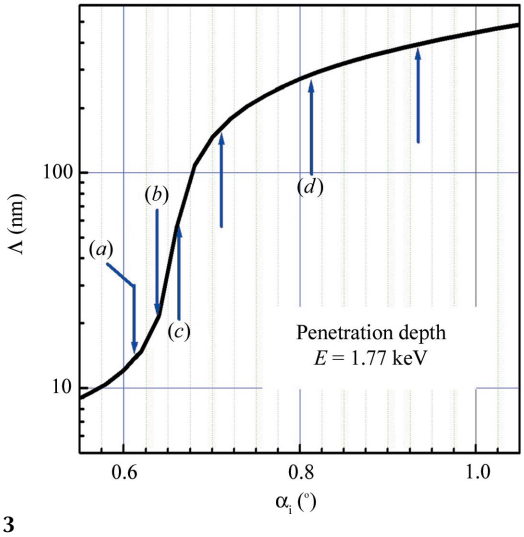

Figure 3
Penetration depth calculated for the present SEBS film. The arrows show the incident angles used in the present measurements.

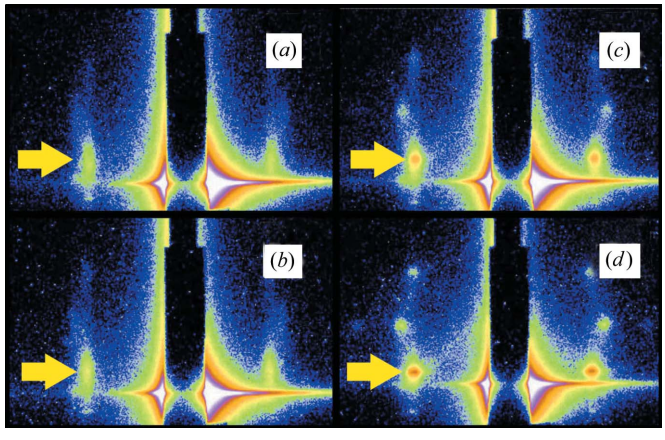

Figure 4
Change of GISAXS profiles with incident angle. The Bragg spot used for the broadening analysis is shown by the arrows.

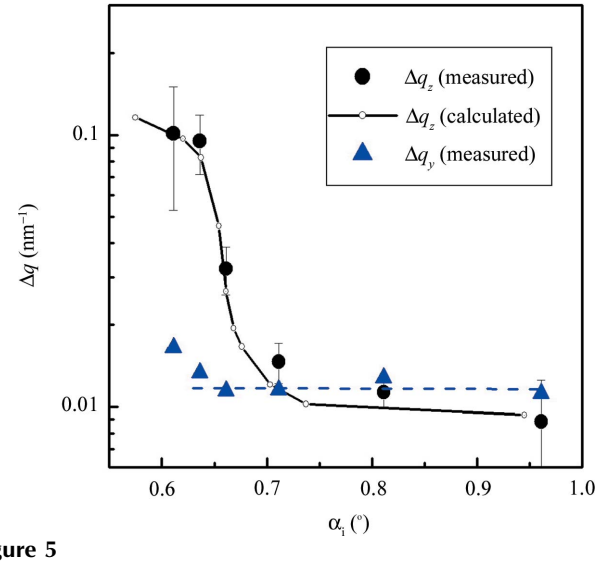

Figure 5
Measured broadening of the Bragg spot in q_z and the corresponding theoretical values as calculated by equation (2). The in-plane width, Δq_y, is almost constant.

$$I(\mathbf{q}) = \overline{F}^2(|\mathbf{q}|)\left[\sum \exp(iq_z z_m)\exp(-z_m/2\Lambda)\right] \times \left[\sum \exp(-iq_z z_n)\exp(-z_n/2\Lambda)\right], \quad (2)$$

where $\overline{F}^2(\mathbf{q})$ is the square-averaged form factor of the spherical core formed by microphase separation with a core radius of 8 nm, $z_{m(n)}$ is the depth of the $m(n)$th lattice plane of the microphase separation structure, Λ is the penetration depth calculated from equation (1) and q_z is the z component of the scattering vector. The FWHMs in the q_z direction calculated for the penetration depth, Λ, given by equation (1) are also plotted in Fig. 5. The calculated width agrees well with the experimental value, leading to the conclusion that the broadening of the Bragg spot in the direction perpendicular to the substrate is explained by the size effect determined by the penetration depth, *i.e.* a depth-resolved GISAXS pattern is obtained. The width in the in-plane direction, Δq_y, is corrected for the beam size assuming that the diffraction spot is a Gaussian and the incident beam is approximated by a Heaviside function whose size was measured by a burn film (P8103 supplied by GEX Corporation). The FWHM Δq_y is almost constant above the critical angle, suggesting that the average in-plane domain structure does not change in the present sample for the depth above the critical angle.

The change of the peak position for the same peak in the directions perpendicular and parallel to the surface is given in Fig. 6. In the figure, the peak positions were corrected for refraction. The resulting magnitude of the scattering vector was about 0.28 nm^{-1}, which agreed with the reported position of the first diffraction peak of the material measured *via* transmission synchrotron radiation small-angle scattering (Kim *et al.*, 1999). It is clearly seen that the lattice is strongly elongated in the direction perpendicular to the surface, up to 22% from the bulk in the surface region within about 50 nm from the surface, corresponding to about 1.5 times the lattice

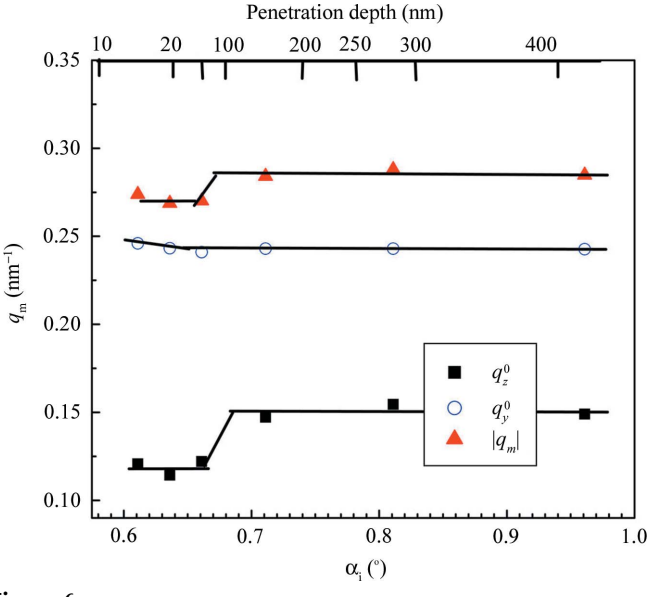

Figure 6
The peak position in the perpendicular and in-plane directions. The lattice spacing changes near the surface. $|q_m| = (q_y^2 + q_z^2)^{1/2}$. Lines are intended to guide the eyes.

constant of the b.c.c. lattice of spherical microphase-separated SEBS8. The in-plane lattice spacing decreased very slightly, in contrast, by about 2.5%. The change of the peak positions for a small angle of incidence may also affect the peak broadening. However, the experimental peak broadening in q_z, about 0.1 nm^{-1} for the surface region, is much larger than the maximum peak shift in q_z observed at the detector for the lowest angle of incidence, about 0.006 nm^{-1}. Therefore, it is concluded that the lattice distortion near the surface does not make a substantial contribution to the present peak broadening. Considering that the FWHM for the q_y direction slightly increases near the surface, yet remains much lower than that for the q_z direction, the effect of disordering should be also marginal for the broadening, although the broadening suggests that the in-plane domain size is smaller at the surface. Concerning the lattice constant, a clear elongation of the lattice was observed at the surface, mostly in the out-of-plane direction. This suggests that the uppermost layer is disturbed by the image force and surface disordering. This suggestion is consistent with the fact that a well defined lattice microstructure is observed by cross-sectional transmission electron microscopy for the same material (Kim *et al.*, 1999), while scanning probe microscopy images at the surface tend to show a more disordered morphology (Sakurai *et al.*, 2005).

4. Conclusions

Depth-sensitive GISAXS measurements have been demonstrated using soft X-rays of 1.77 keV. By examining the broadening of Bragg peaks from self-organized SEBS film samples, depth resolution of a couple of tens of nanometres was confirmed. This resolution is convenient for probing the depth-dependent nanostructures of self-organized polymers, whose unit size is of the order of ten nanometres. The diffraction patterns observed using GISAXS at 1.77 keV were simple because it is possible to control the penetration depth and hence suppress the wave reflected from the Si substrate. Within a couple of lattice planes from the surface, the lattice of spherical cores is elongated in the direction perpendicular to the surface.

Part of the present work has been supported by a Grant-in-Aid for Scientific Research (22651034 by JSPS). HO acknowledges Professor A. Takahara for helpful discussions.

References

Ade, H. & Hitchcock, A. (2008). *Polymer*, **49**, 643–675.
Babboneau, D., Camelio, S., Lantia, D. T., Simonot, L. & Michel, A. (2009). *Phys. Rev. B*, **80**, 155446.
Chantler, C. T., Olsen, K., Dragoset, R. A., Chang, J., Kishore, A. R., Kotochigova, S. A. & Zucker, D. S. (2005). *X-ray Form Factor, Attenuation and Scattering Tables*, http://physics.nist.gov/PhysRefData/FFast/html/form.html.
Harrison, C., Dagata, J. & Adamson, D. H. (2004). *Developments in Block Copolymer Science and Technology*, edited by I. Hamley, pp. 295–324. Chichester: Wiley.
Huinink, H. P., van Dijk, M. A., Brokken-Xijp, J. C. & Sevink, G. J. A. (2001). *Macromolecules*, **34**, 5325–5330.
Jin, S., Yoon, J., Heo, K., Park, H.-W., Kim, J., Kim, K.-W., Shin, T. J., Chang, T. & Ree, M. (2007). *J. Appl. Cryst.* **40**, 950–958.

Kim, J.-K., Lee, H. H., Sakurai, S., Aida, S., Masamoto, J., Nomura, S., Kitragawa, Y. & Suda, Y. (1999). *Macromolecules*, **32**, 6707–6717.
Kuhlmann, M., Feldkamp, J. M., Patommel, J., Roth, S. V., Timmann, A., Gerhke, R., Müller-Buschbaum, P. & Schroer, C. G. (2009). *Langmuir*, **25**, 7241–7243.
Matsen, M. W. & Bates, F. S. (1996). *Macromolecules*, **29**, 7641–7644.
Mukhopadhyay, M. K., Lurio, L. B., Jiang, Z., Jiao, X., Sprung, M., DeCaro, C. & Sinha, S. K. (2010). *Phys. Rev. E*, **82**, 011804.
Müller-Buschbaum, P., Gutmann, J. S., Cubitt, R. & Stamm, M. (1999). *Colloid Polym. Sci.* **277**, 1193–1199.
Naudon, A., Babboneau, D., Thiaudiere, D. & Lequien, S. (2000). *Physica B*, **283**, 69–74.
Okuda, H., Kato, M., Ochiai, S. & Kitajima, Y. (2009). *Appl. Phys. Express*, **2**, 126501.
Park, I., Park, S., Park, H.-W., Chang, T., Yang, H. & Ryu, C. Y. (2006). *Macromolecules*, **39**, 315–318.
Park, S., Wang, J.-Y., Kim, B., Chen, W. & Russel, T. (2007). *Macromolecules*, **40**, 9059–9063.
Perlich, J., Rubeck, J., Botta, S., Gehrke, R., Roth, S. V., Ruderer, M. A., Prams, S. M., Rawolle, M., Zhong, Q., Körstgens, V. & Müller-Buschbaum, P. (2010). *Rev. Sci. Instrum.* **81**, 105105.
Rauscher, M., Salditt, T. & Spohn, H. (1995). *Phys. Rev. B*, **52**, 16855–16863.
Roth, S. V., Autenrieth, T., Gruebel, G., Riekel, C., Burghammer, M., Hengstler, R., Schultz, L. & Mueller-Buschbaum, P. (2007). *Appl. Phys. Lett.* **91**, 0091915.
Roth, S. V., Burghammer, M., Riekel, C., Müller-Buschbaum, P., Diethert, A., Panagiotou, P. & Walter, H. (2003). *Appl. Phys. Lett.* **82**, 1935–1937.
Sakurai, S., Sakamoto, A., Itaya, A., Yamada, K., Mouri, E. & Matsuoka, H. (2005). *Int. J. Appl. Chem.* **1**, 1–11.
Sasaki, S., Masunaga, H., Tajiri, H., Inoue, K., Okuda, H., Noma, H., Honda, K., Takahara, A. & Takata, M. (2007). *J. Appl. Cryst.* **40**, s642–s644.
Singh, M. A. & Groves, M. N. (2009). *Acta Cryst.* A**65**, 190–201.
Smilgies, D., Busch, P., Papadakis, C. M. & Possett, D. (2002). *Synchrotron Rad. News*, **5**, 35.
Tolan, M. (1999). *X-ray Scattering from Soft-Matter Thin Films.* Berlin: Springer Verlag.
Turner, M., Rubinstein, M. & Marques, C. M. (1994). *Macromolecules*, **27**, 4986–4992.
Wang, C., Araki, T. & Ade, G. (2005). *Appl. Phys. Lett.* **87**, 214109.